A&A 548, A72 (2012)
DOI: 10.1051/0004-6361/201220120

Astronomy & Astrophysics

Observational constraints for the circumstellar disk of the B[e] star CPD−52 9243⋆

L. S. Cidale[1,⋆⋆], M. Borges Fernandes[2], I. Andruchow[1,⋆⋆], M. L. Arias[1,⋆⋆], M. Kraus[3], O. Chesneau[4], S. Kanaan[5], M. Curé[5], W. J. de Wit[6], and M. F. Muratore[1,⋆⋆⋆]

[1] Departamento de Espectroscopía, Facultad de Ciencias Astronómicas y Geofísicas, Universidad Nacional de La Plata, and Instituto de Astrofísica La Plata, CCT La Plata, CONICET Paseo del Bosque S/N, B1900FWA, La Plata, Argentina
e-mail: lydia@fcaglp.fcaglp.unlp.edu.ar
[2] Observatório Nacional – MCTI, Rua General José Cristino 77, 20921–400 São Cristovão, Rio de Janeiro, Brazil
[3] Astronomický ústav, Akademie věd České Republiky, Fričova 298, 25165 Ondřejov, Czech Republic
[4] Laboratoire Lagrange, UMR7293, Université de Nice Sophia-Antipolis, CNRS, Observatoire de la Côte d'Azur, 06300 Nice, France
[5] Departamento de Física y Astronomía, Facultad de Ciencias, Universidad de Valparaíso, Av. Gran Bretaña 1111, 5030 Casilla Valparaíso, Chile
[6] European Southern Observatory, 3107 Alonso de Cordova, Vitacura, Santiago, Chile

Received 28 July 2012 / Accepted 3 October 2012

ABSTRACT

Context. The formation and evolution of gas and dust environments around B[e] supergiants are still open issues.
Aims. We intend to study the geometry, kinematics and physical structure of the circumstellar environment (CE) of the B[e] supergiant CPD−52 9243 to provide further insights into the underlying mechanism causing the B[e] phenomenon.
Methods. The influence of the different physical mechanisms acting on the CE (radiation pressure, rotation, bi-stability or tidal forces) is somehow reflected in the shape and kinematic properties of the gas and dust regions (flaring, Keplerian, accretion or outflowing disks). To investigate these processes we mainly used quasi-simultaneous observations taken with high spatial resolution optical long-baseline interferometry (VLTI/MIDI), near-IR spectroscopy of CO bandhead features (Gemini/Phoenix and VLT/CRIRES) and optical spectra (CASLEO/REOSC).
Results. High angular resolution interferometric measurements obtained with VLTI/MIDI provide strong support for the presence of a dusty disk(ring)-like structure around CPD−52 9243, with an upper limit for its inner edge of ∼8 mas (∼27.5 AU, considering a distance of 3.44 kpc to the star). The disk has an inclination angle with respect to the line of sight of 46 ± 7°. The study of CO first overtone bandhead evidences a disk structure in Keplerian rotation. The optical spectrum indicates a rapid outflow in the polar direction.
Conclusions. The IR emission (CO and warm dust) indicates Keplerian rotation in a circumstellar disk while the optical line transitions of various species are consistent with a polar wind. Both structures appear simultaneously and provide further evidence for the proposed paradigms of the mass-loss in supergiant B[e] stars. The presence of a detached cold CO ring around CPD–52 9243 could be due to a truncation of the inner disk caused by a companion, located possibly interior to the disk rim, clearing the center of the system. More spectroscopic and interferometric data are necessary to determine a possible binary nature of the star.

Key words. supergiants – stars: winds, outflows – stars: mass-loss – circumstellar matter – stars: individual: CPD-52 9243

1. Introduction

B[e] supergiants (sgB[e]s) are massive and luminous evolved B-type stars that show the B[e] phenomenon (Lamers et al. 1998). However, their stellar fundamental parameters and position in the Hertzsprung-Russell (HR) diagram (in a pre- or post-red supergiant phase) are still poorly known due to the uncertainties in distance determination and the complexity of the observed spectral features.

SgB[e] stars exhibit a hybrid spectrum which is characterized by both: i) in the optical region, the presence of strong P Cygni profiles in the Balmer lines, and narrow low-excitation permitted and forbidden emission lines from singly ionized and neutral metals; and ii) in the UV region, the presence of broad absorption features of higher-excitation levels of highly ionized metals. In addition, they also present a strong near/mid-infrared excess due to hot circumstellar dust (Zickgraf 1998). Thus, to describe the hybrid spectrum observed in the sgB[e]s, Zickgraf et al. (1985) proposed an empirical model, called "the two-component wind", which consists of a hot and rapid line driven wind in the polar regions, and a slow, cool and dense wind in the equatorial zones, where dust could be formed. The presence of non-spherical circumstellar environments (CE) around these stars was also suggested by polarimetric and spectro-polarimetric data (Magalhães 1992; Oudmaijer & Drew 1999; Melgarejo et al. 2001; Magalhães et al. 2006).

⋆ Based on observations taken with: 1) Telescopes at Paranal ESO Observatory under the program 085.D–0454 and 385.D–0513A; 2) Gemini South/Phoenix instrument, science program GS-2010A-Q-41; 3) J. Sahade Telescope at Complejo Astronómico El Leoncito (CASLEO), operated under an agreement between the Consejo Nacional de Investigaciones Científicas y Técnicas de la República Argentina, the Secretaría de Ciencia y Tecnología de la Nación and the National Universities of La Plata, Córdoba and San Juan.
⋆⋆ Member of the Carrera del Investigador Científico, CONICET, Argentina.
⋆⋆⋆ Research Fellow of the Universidad Nacional de La Plata, Argentina.

However, this circumstellar scenario was really proved for the star CPD−57 2874, thanks to the high angular resolution provided by the optical long-baseline interferometry, using the Very Large Telescope (VLT, Domiciano de Souza et al. 2007).

The mechanisms that lead to the formation of a disk of gas and dust are still under debate. In order to explain the origin and physical properties of these structures different models have been suggested: 1) wind compressed disks (Bjorkman & Cassinelli 1993); 2) viscous Keplerian rotating disks (Porter 2003); 3) enhanced mass flux and slow wind speed associated to the centrifugally reduced effective gravity near the equator (Pauldrach et al. 1986); 4) slow wind solutions derived from high-rotating line driven winds with rotation velocities greater than 70% of the critical rotation velocity (Curé 2004); 5) enhanced mass loss from a bi-stability zone triggered by the change, from the equator to the pole, of the radiation temperature, i.e.: the optical depth, and the spectral lines that drive the wind (Lamers & Pauldrach 1991; Curé et al. 2005); 6) binarity, since some sgB[e] candidates are suggested to be in binary systems (Miroshnichenko 2006).

The influence of the different physical mechanisms acting on the CE (radiation pressure, rotation, bi-stability or tidal forces) is somehow reflected in the shape, kinematic and radial density structure of the gas and dust regions (flaring, Keplerian, accretion or outflowing disks). Therefore, we intend to study these regions based on: i) interferometry techniques, which provide strong support for the presence of a disk-like structure; and ii) emission from molecules, that can be used to trace the outermost region of the gaseous CE and its kinematics. Particularly, the structure of CO first overtone bandhead, arising at 2.3 μm, is extremely sensitive to the motion of a warm disk and is a very good discriminator between Keplerian rotating disks and outflowing disks surrounding sgB[e]s (see Kraus 2009).

Therefore, in order to better understand the circumstellar scenario around sgB[e]s, we studied the emission-line star CPD−52 9243, which has been classified as a sgB[e] candidate (Winkler & Wolf 1989; Miroshnichenko et al. 1995; Lamers et al. 1998; Kraus 2009), combining quasi-simultaneous spectroscopic observations around the Hα and near-IR region with optical long-baseline interferometric data.

In Sect. 2 we present our observations and data reduction; a summary of the current knowledge of this star and the results of our study are shown in Sect. 3; our discussion and conclusions are given in Sect. 4.

2. Observations

We obtained quasi-simultaneous observations of CPD−52 9243 in the optical, near-IR and mid-IR, using spectroscopy and high angular resolution interferometry in April and May 2010. Tables 1 and 2 list the logs of observations.

2.1. The optical spectrum

Two optical spectra of CPD−52 9243 were taken at the Complejo Astronómico El Leoncito (CASLEO), San Juan, Argentina, in 2010, May 23 and 25, with the Cassegrain echelle REOSC spectrograph attached at the 2.15-m telescope. The adopted instrumental configuration was: a 400 mm^{-1} grating in cross dispersion mode, a slit-width of 250 μm and a Tek 1024 × 1024 CCD detector. The covered spectral region ranges from 4800 Å to 6700 Å with a mean resolution R = 13 000 (see Table 1). Data reduction and wavelength calibration were performed using the IRAF[1] software package.

Table 1. Log of the spectroscopic observations of CPD−52 9243 in the optical and near-IR wavelength ranges.

Date	Spectral range [μm]	R	Observatory/ Instrument
2010–04–03	2.321–2.329	50 000	Gemini/Phoenix
2010–04–06	2.310–2.330	50 000	ESO/CRIRES
2010–05–23	0.480–0.670	13 000	CASLEO/REOSC
2010–05–25	0.480–0.670	13 000	CASLEO/REOSC

Table 2. VLTI/MIDI observing log for CPD−52 9243.

Baseline	Date	t_{obs} UTC	UT baseline	B_p [m]	PA [°]
B1	2010–04–26	08:47:26	UT2–UT3	36.9	64.3
B2	2010–04–27	08:45:43	UT3–UT4	61.9	136.1
B3	2010–05–26	02:33:24	UT3–UT4	55.3	84.8
B4	2010–05–30	01:23:44	UT3–UT4	46.1	14.3

2.2. Near-infrared spectroscopy

2.2.1. Gemini/Phoenix observations

Near-IR observations of CPD−52 9243 were acquired in service mode in 2010, April 3, with Phoenix; a cryogenic, long slit, high resolution infrared spectrograph mounted as a visitor instrument on the 8-m Gemini South telescope in Chile.

Phoenix used an Aladdin 512 × 1024 InSb array as a detector and a 4 pixel wide slit was selected. High resolution spectra (R ∼ 50 000) were taken using the K4308 filter centered at 2.323 μm in order to observe the CO molecular bandhead. The covered wavelength range was 2.319–2.329 μm. Observations were taken with the offset pattern ABBA along the slit, in order to remove the sky emission. All reductions were performed using IRAF software package routines. The reduction steps were based on the example available at NOAO webpages[2]. We performed the telluric correction by taking the ratio of the spectrum of CPD−52 9243 with that of a B9V telluric standard star. The telluric standard star HIP 84690 was observed immediately before the science target, close in airmass. We selected a late B-type telluric standard star because its spectrum only exhibits hydrogen lines.

In order to construct a flux-calibrated spectrum, we inspected the public available photometric data from the 2MASS and MSX missions to obtain information of the shape of the underlying continuum in the CO band region. The photometric data indicate a linearly slightly rising continuum with wavelength. Then, we interpolated the photometric continuum flux over the CO band spectrum. From model calculations of the CO bands it turned out that the only reliable continuum position in the observed spectrum is on the short-wavelength edge of the spectrum, between the well-resolved lines from the first CO band.

[1] IRAF is distributed by the National Optical Astronomy Observatories, which is operated by the Association of Universities for Research in Astronomy (AURA) under cooperative agreement with the National Science Foundation.

[2] http://www.noao.edu/ngsc/phoenix/phoenix.html

2.2.2. VLT/CRIRES observations

A spectrum of CPD−52 9243 was also taken in 2010, April 6, with the near-IR cryogenic high resolution spectrograph CRIRES mounted on UT1 of the VLT (Kaeufl et al. 2004). The target was part of a sample of sixteen well-known, K-band bright sgB[e] stars and candidates, which were observed in order to study in detail the kinematic signature of the CO first overtone bandhead (Muratore et al., in prep.). Observations were executed with a slit width of 0.4″ delivering a spectral resolution R of approximately 50 000 (or 6 km s^{-1}). The covered wavelength range was 2.276–2.326 μm. A standard nodding on-slit strategy was applied to remove sky and detector glow, without AO correction. A small jittering offset at each nod position was also applied to better remove bad pixels. The DIT was chosen bearing in mind the non-linearity regime of the CRIRES InSb Aladdin III detectors. A telluric standard was taken immediately after the science targets, close in airmass; no particular care was taken to correct for the small difference in airmass between science and telluric standard as the telluric correction was found satisfactory. The seeing conditions were excellent with a median seeing of 0.6″ delivering a signal-to-noise ratio of ∼100. The presented CRIRES spectrum was reduced with the CRIRES pipeline provided by ESO and was normalized to the continuum flux level. The flux calibration was performed the same way as for the Phoenix spectrum.

2.3. Interferometric observations

The interferometric observations of CPD−52 9243 were carried out at Paranal ESO Observatory in service mode with MIDI, the mid-infrared instrument of the VLT interferometer (Leinert et al. 2004), on different nights during April and May, 2010. The N-band spectrum as well as the spectrally dispersed fringes were recorded between 8 μm and 13 μm with a spectral resolution of R = 30 using a prism. In order to study the wavelength dependence of the object apparent size, a total of 4 data sets have been obtained with UT2-UT3 and UT3-UT4 baselines using the SCI-PHOT mode. The projected baselines range from 35 m to 65 m, for different orientations on the sky plane. Table 2 presents the log of the interferometric observations: dates and Universal Time Coordinated (UTC) of the observations, baseline configuration, projected baseline length (B_p) and position angle (PA). The UV-plane coverage is shown in Fig. 1.

HD 152980 was observed as a calibrator star. The flux of this star at [12]-band is 22.03 Jy[3], and its angular diameter is θ_{UD} = 3.64 ± 0.12 mas[4]. Data reduction was carried out with MIA+EWS data reduction package (Jaffe 2004; Leinert et al. 2004).

3. Results

3.1. Stellar parameters and distance

CPD−52 9243 (Hen 3-1138, α_{2000} = 16^{h}07^{m}02^s.03 and δ_{2000} = −53°03′45.4″, V = 10.3 mag and K = 4.4 mag) exhibits a visual photometric variability. The V light curve of CPD−52 9243, downloaded from the All Sky Automated Survey (ASAS) catalogue[5], shows irregular light variations with amplitudes up to 0.2 mag. We performed period analysis with the *Period* 4 code (Lenz & Breger 2005). Although we were unable to find reliable periods to describe the variation, a medium-term variation (of hundreds of days) could be present.

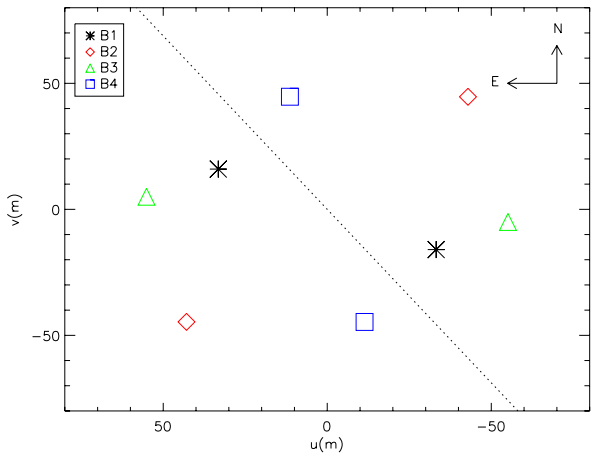

Fig. 1. The UV-plane coverage of CPD−52 9243 obtained with VLTI/MIDI. The dotted line represents the polarization angle measured by Swings (1981).

Swings (1981) classified CPD−52 9243 as B8 Ia and, using the Na I interestellar absorption lines, estimated a distance from the Sun of about 3.1 kpc and an extinction $A_V \sim 4.5$. In addition, McGregor et al. (1988) derived the following stellar parameters: log T_{eff} = 4.2 and log $L/L_\odot$ = 5.4, while Kozok (1985), using UBV reddening-free color and magnitudes of Be stars, adopted a M_V = −6.6 for this star and estimated a distance of 2.14 kpc.

The optical high-resolution spectra of this star was described by Swings (1981), Winkler & Wolf (1989) and Lopes et al. (1992). The star shows strong Balmer lines with P Cygni profiles, with a separation between emission and absorption components of 145 km s^{-1}. The spectrum is also crowded with emission lines of singly ionized atoms, and the stronger ones have P Cygni profiles too. He I appears only in absorption and the two unique emission forbidden lines observed in the optical spectrum are [O I] $\lambda\lambda$6300, 6364 Å (Swings 1981). This star also displays CO emission bands, which were reported by Whitelock et al. (1983) and McGregor et al. (1988). Brγ and Paβ are also present in the spectrum as weak emission lines. A strong polarization, P = 5%, with a polarization angle of 36° was reported by Swings (1981).

Our optical spectrum is quite similar to those reported previously in the literature. It displays mainly H I and Fe II lines with P Cygni profiles (see Fig. 2). The Na I lines show a complex structure. From the absorption component of the P Cygni lines we derived an outflowing projected velocity of about −200 km s^{-1}. The peak of the emission component of the P Cygni profiles has a velocity of –54 km s^{-1}. Considering this value as the systemic velocity of the star (see discussion in Sect. 3.3), and taking into account that this object is located in the galactic plane: l = 329.86 and b = −0.74, we can derive a kinematical distance assuming circular orbits for the gas and stars around the galactic center. We made use of the galactic rotation curve derived for the fourth quadrant by McClure-Griffiths & Dickey (2007) and we obtained a distance of 3.44 ± 0.8 kpc from the Sun. Then, considering the color excess, $E(B-V)$ = 1.74, derived by Borges Fernandes et al. (in prep.) from the analysis of diffuse interstellar bands (DIBs), we obtained a mean absorption A_V = 5.39 mag, and the corresponding absolute

[3] Data taken from http://nsted.ipac.caltech.edu/index.html

[4] θ_{UD} was obtained from the calibrators list provided by MIA+EWS data reduction package.

[5] http://www.astrouw.edu.pl/asas/

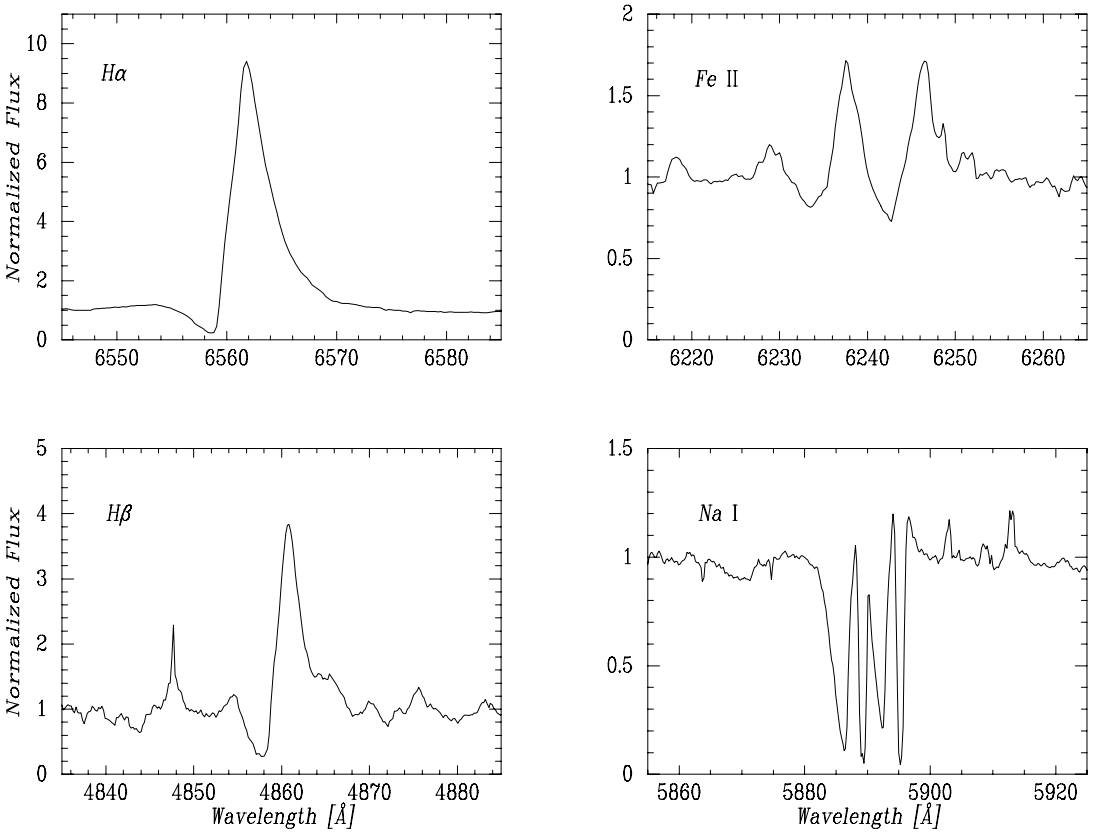

Fig. 2. P Cygni line profiles of Hα, Hβ, Fe II (74) $\lambda\lambda$6238, 6247 and Na I (1) $\lambda\lambda$5890, 5896.

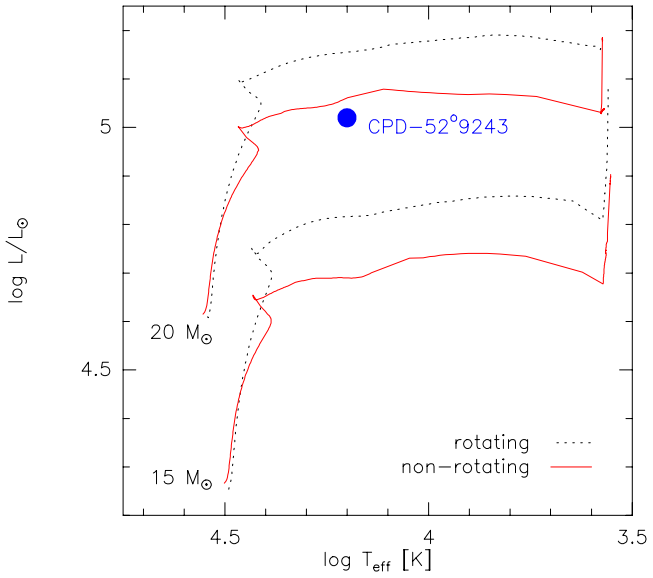

Fig. 3. HR diagram for CPD−52 9243 together with the evolutionary tracks from Ekström et al. (2012).

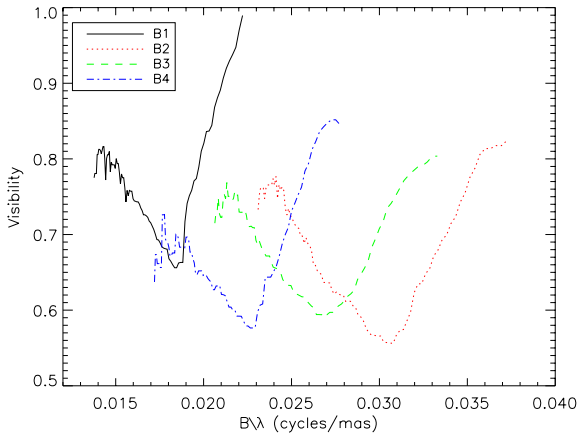

Fig. 4. VLTI/MIDI calibrated visibility curves of CPD−52 9243 as a function of the spatial frequency B/λ.

magnitude and luminosity, $M_V = -7.70$ mag and $\log L/L_\odot = 4.97$. These values agree very well with those derived by Swings (1981) and McGregor et al. (1988). Finally, from our data set we can locate the star in the HR diagram (see Fig. 3) and determine the stellar mass considering the newly evolutionary tracks computed by Ekström et al. (2012). The values derived for the current stellar mass are 17.4 ± 1.0 and 18.6 ± 0.5 solar masses, assuming rotating ($V \sin i/V_{\rm crit} = 0.4$) and non-rotating evolutionary models, respectively.

3.2. Disk size and inclination

N-band calibrated visibility curves of CPD−52 9243, as function of wavelength, were taken using VLTI/MIDI for different baselines and position angles (see Fig. 4 and Table 2). The object is clearly resolved for all baselines and there is a decrease in the value of the visibility with wavelength, followed by a subsequent increase. The spectral flux for the different baselines is shown in Fig. 5. In all baselines, it is possible to see the presence of a more extended envelope around 10 μm, corresponding to the silicate bands, which has an opacity higher than that of the continuum. The silicate bands are also seen when combining spectra obtained by VLTI/MIDI and *Spitzer* (see Fig. 6). MIDI and *Spitzer* observations agree very well. The estimated error values are between 10% to 20% of the fluxes.

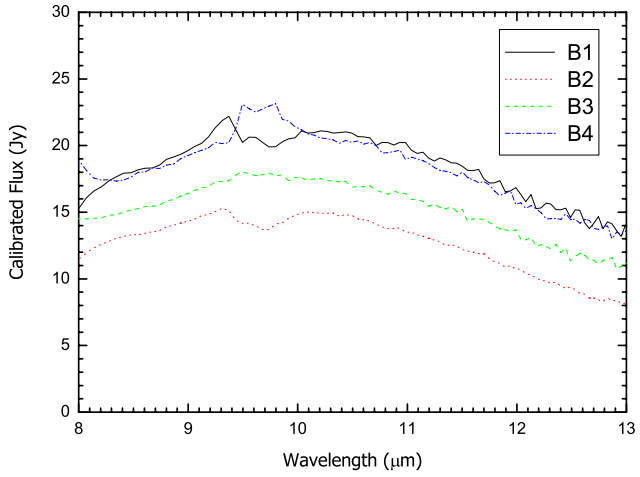

Fig. 5. VLTI/MIDI calibrated flux for CPD-52 9243.

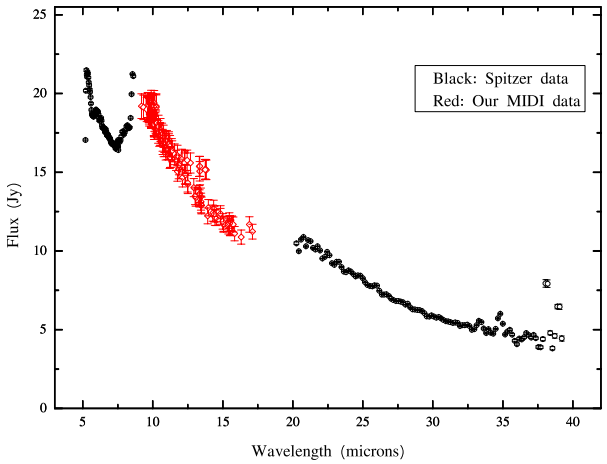

Fig. 6. Spectral flux taken with VLTI/MIDI (red) together with data obtained with *Spitzer* (black). Both spectra reveal the presence of the silicate bands in emission.

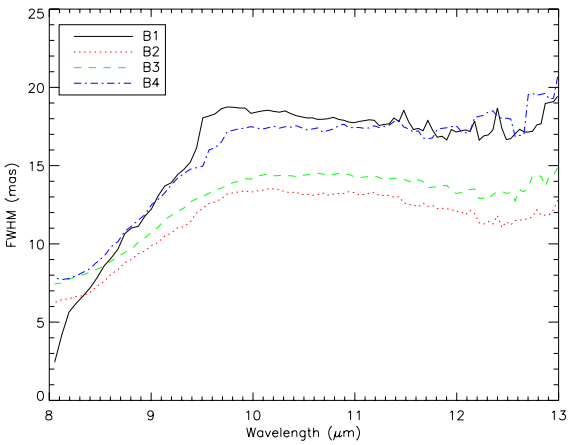

Fig. 7. The CE extension obtained from the visibilities of each VLTI/MIDI baseline.

Considering a (1D or round) Gaussian distribution (Leinert et al. 2004), we calculated the full width at half maximum (FWHM) from the observed visibilities for each baseline. Figure 7 shows the FWHM values (listed in Table 3) as a function of wavelengths. All curves present a similar behavior: a rapid increase of the extension from 8 to 10 μm followed by a flat slope. This behavior is due to the increase of opacity of the silicate feature around 10 μm. However, the CE extension does not drop back with the subsequent decrease of this opacity at 11–13 μm, because it is compensated by an increase of the continuum opacity due to the presence of cooler dust in more extended regions.

There is also a consistent increase of the FWHM, especially for baselines with position angles close to the polarization angle. This variation of extension as a function of the baseline projection (PA) agrees with a non-spherically symmetric circumstellar geometry for CPD-52 9243. Assuming, for example, a disk geometry, the baselines presenting a larger FWHM would be orientated close to its major axis. In addition, the alignment of the polarization angle with the major axis of the disk would indicate the presence of optically thick circumstellar material. On the other hand, a major axis perpendicular to the polarization angle would indicate an optically thin medium (Angel 1969; Brown & McLean 1977).

We also modeled the observed visibilities, considering a simple scenario for the circumstellar medium, with an elliptical Gaussian distribution. The model fitting is done by minimizing the chi-square (χ^2) on the visibilities, using a Levenberg-Marquardt (LM) two-dimensional algorithm. For this model, the star does not contribute to the N-band emission, thus all the flux comes from the circumstellar dusty environment. This model has three free parameters: (i) the FWHM of the major axis; (ii) the flattening, i.e., the ratio of the FWHM of the minor axis and of the major axis; and (iii) the orientation of the major axis on the plane of the sky (θ).

Table 3. FWHM for each combination of baseline and position angle (see Table 2) for CPD−52 9243.

λ μm	$FWHM_{B1}$ [mas]	$FWHM_{B2}$ [mas]	$FWHM_{B3}$ [mas]	$FWHM_{B4}$ [mas]
8.12	6.15	6.31	6.77	7.92
8.33	8.87	6.09	7.31	7.55
8.54	10.32	7.42	7.84	8.98
8.74	11.59	8.56	8.83	10.54
8.94	12.68	9.47	9.88	11.90
9.13	14.14	10.29	11.03	13.25
9.32	15.73	10.71	11.88	14.16
9.51	18.15	12.03	12.54	14.76
9.69	18.79	12.72	13.09	16.39
9.86	18.74	13.00	13.63	17.25
10.04	18.16	12.89	13.89	17.30
10.20	18.31	13.05	13.97	17.34
10.37	18.27	13.13	13.91	17.41
10.53	18.60	13.03	13.96	17.11
10.69	18.48	13.08	13.97	17.08
10.84	18.29	13.08	14.04	17.38
10.99	17.88	13.04	13.94	17.19
11.14	17.89	12.93	13.97	17.09
11.29	17.63	12.83	13.78	17.21
11.43	17.98	12.51	13.84	17.49
11.57	17.52	12.39	13.67	16.82
11.72	17.53	12.48	13.42	16.71
11.86	16.73	12.40	13.44	17.33
11.99	18.11	11.75	12.84	17.26
12.13	17.96	11.98	13.30	17.29
12.27	18.13	11.17	12.66	17.69
12.40	19.32	11.57	12.88	18.10
12.53	17.54	11.41	12.72	17.24
12.66	17.95	11.85	12.87	17.69
12.79	18.21	12.22	13.72	19.19
12.91	19.31	11.76	13.77	19.36

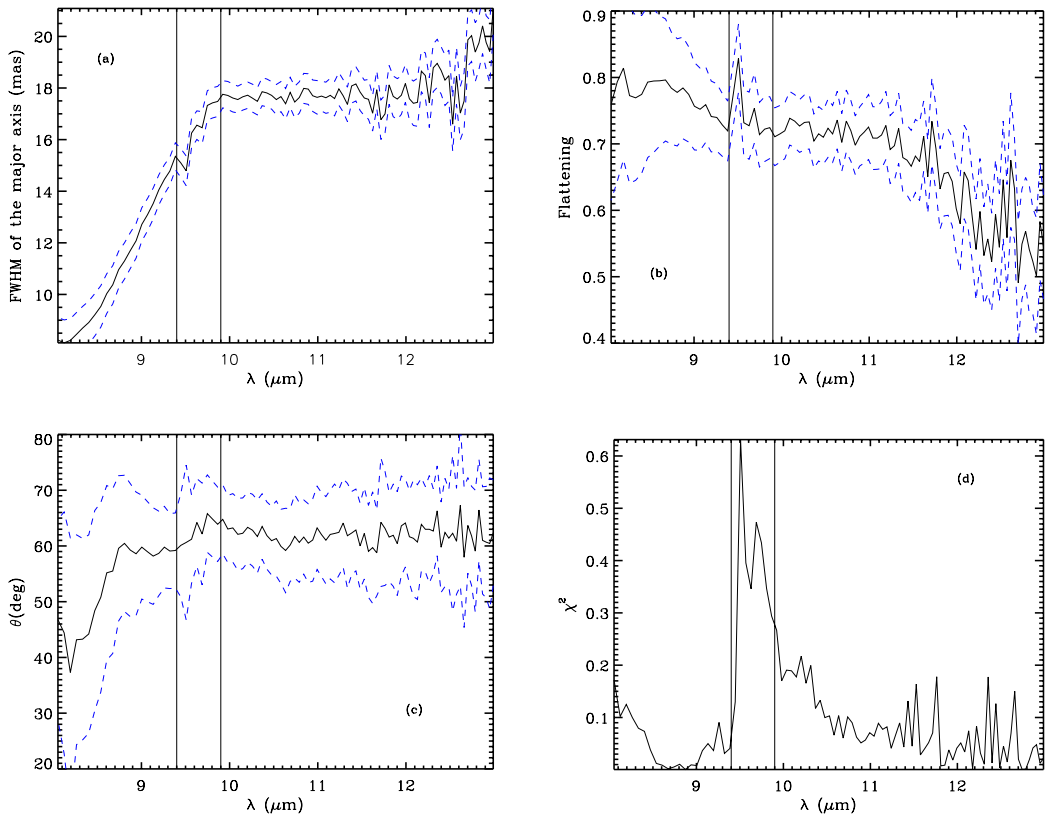

Fig. 8. The parameters provided by the best model, obtained by fitting an elliptical Gaussian distribution to MIDI visibilities, as a function of wavelength: **a)** the FWHM of the major axis; **b)** the flattening (ratio of the FWHM of the minor axis to that of the major axis); **c)** the projection of the major axis (θ) on the sky plane; and **d)** the χ^2 for each wavelength. The dashed lines indicate the errors for each parameter as a function of the wavelength. The vertical solid lines represent the atmospheric ozone band.

Since the CE extension varies within the *N*-band, we assume that the free parameters are also wavelength dependent. In Fig. 8, we show the best-fit model parameters and the χ^2 values. The low χ^2 for all wavelengths needs to be taken with caution due to the very few baselines and free parameters to be modeled. The increase of the χ^2, seen in the panel (d) of Fig. 8, around 9.6 μm, is due to the presence of the atmospheric ozone band. The region from 12.5 μm to 13.5 μm is also affected by photometric calibration issues, increasing the noise and also biasing the visibilities toward higher values. This explains the oscillations seen in all panels of Fig. 8. The flattening coefficient in this region should be taken with more caution. Considering the mean value of each parameter (presented in Table 4), we can see the presence of a disk structure with the FWHM of the major axis around 16 mas. This would also mean an upper limit for the inner dusty disk of about 8 mas, since warm dust, and not hot dust, is the main responsible by *N*-band emission. Based on the mean flattening and its error, obtained by our model fitting, we see that the system has a mean disk inclination of 46 ± 7°. The geometrical simple model is shown in Fig. 9.

In addition, our best model considers θ around 60°. This result is also consistent with the FWHM obtained by the simple Gaussian distribution, as can be seen in Fig. 7. However, we cannot consider neither a parallel nor a perpendicular alignment to the large polarization source reported by Swings (1981). This may be happening due to the absence of the correction of the interstellar polarization by these authors and also because we are modeling just four baselines. Thus, definitely more baselines are necessary to better constrain these parameters, by using not only geometrical models, but also physical models.

Table 4. Parameters of our best-fitting disk model.

FWHM major axis (mas)	16.35 ± 0.73
Flattening	0.69 ± 0.07
θ (°)	60.13 ± 9.57
χ^2	0.10

3.3. CO band emission

We present the *K*-band spectrum obtained with the CRIRES and Phoenix spectrographs, which cover, respectively, the wavelength regions of the first and second bandhead of the CO first overtone bands at 2.2935 μm and 2.3227 μm (rotational-vibrational transitions $v = 2 \rightarrow 0$ and $v = 3 \rightarrow 1$, where v is the vibrational quantum number). The flux-calibrated CO spectrum was dereddened using the color excess adopted in Sect. 3.1. The pure (i.e. continuum subtracted) CO spectrum resulting from this procedure is shown in Fig. 10 (top panel). Some individual non-blended lines from the first band (rotational-vibrational transitions $v = 2 \rightarrow 0$) are visible at the short-wavelength edge of the Phoenix spectrum (<2.3224 μm).

The individual rotational-vibrational CO emission lines are clearly double-peaked, indicating either rotation in a quasi-Keplerian disk, or an outflow confined within some solid angle around the equatorial plane, which results in a slow, high-density disk-like outflow ("the two-component wind"). The latter was confirmed to be a natural outcome of hydrodynamical wind calculations, the so-called Ω-slow wind solution, found by Curé (2004) and Curé et al. (2005).

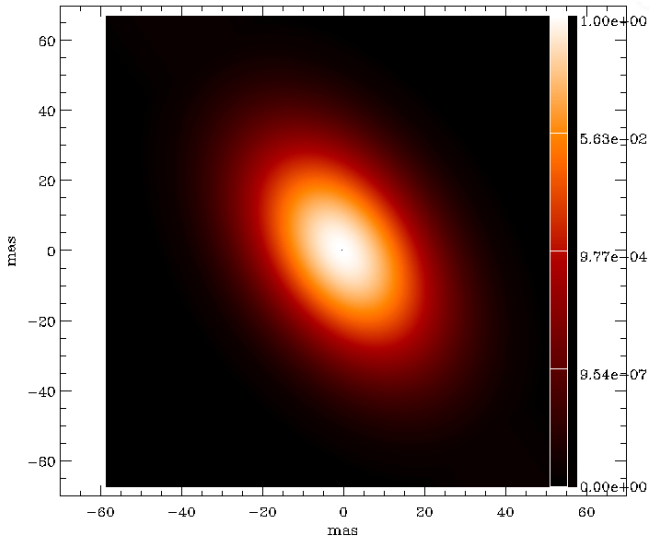

Fig. 9. The geometrical model of the CE of CPD−52 9243 considering an elliptical Gaussian distribution.

With respect to the kinematics seen in the lines forming the CO bands, these two scenarios (Keplerian disk and outflowing disk-forming wind) are, however, indistinguishable at first. This is because the CO emission is usually generated in a narrow ring region in which the velocity can be assumed constant. Hence both rotation and (constant) outflow scenarios deliver the same double-peaked profile. However, only if the distance of the emitting CO gas from the star is known it will be possible to determine which scenario better applies, since the rotation velocity will decrease with distance, while the slow outflowing wind will increase with radius and then settle at its terminal velocity.

The peak separation of the rotational-vibrational lines of the $2 \rightarrow 0$ band indicates a maximum radial or rotational velocity, projected to the line of sight, of about 25–26 km s^{-1}. Then, accounting for the disk inclination, $i = 46.1°$, as obtained from the interferometric data (Sect. 3.2), a rotation or outflow velocity of 36 km s^{-1} is obtained. Furthermore, we note a radial velocity shift of the CO spectra of about –55 km s^{-1}, which is in good agreement with the systemic velocity of the star obtained from the emission component of the metal and Balmer lines (Sect. 3.1), and therefore can be ascribed to the star's radial velocity.

To fit the CO spectrum we apply the disk code of Kraus et al. (2000). The CO gas is assumed to be in LTE, which is a reasonable assumption considering the high densities in circumstellar disks. Optical depth effects in the CO bands are taken into account, and the kinematics in the disk (Keplerian rotation or constant velocity outflow, respectively) are represented by a double-peaked profile function in which each contributing CO ro-vibrational line has been folded. From our experience with CO band modeling, we know that it is sufficient to consider a narrow ring with constant CO column density and temperature (see, e.g., Kraus et al. 2000; Kraus 2009; Liermann et al. 2010). This ring can be interpreted as the inner edge of the molecular disk or outflow region, because this region has the highest temperature and density, hence dominating completely the emission spectrum.

Our model calculations covered a large range of temperatures and densities, while the ring inclination was kept fixed at the value of $i = 46 \pm 7°$ as provided by the interferometric data for the dusty disk. The velocity structure that better reproduce the shape (width and peak-separation) of the resolved lines at the short-wavelength end of the spectrum is for a rotational velocity of 36 ± 4 km s^{-1}. This value, once determined, was further also kept fix.

The best-fitting model (see Fig. 10, bottom panel) agrees excellently with observations. The parameters obtained for the disk are listed in Table 5. The quantity listed in the last column is the area, A_{CO}, of the emitting ring, which was computed using the factor needed to fit the computed flux to the observed one, and assuming a distance to the star of 3.44 ± 0.8 kpc. To place the CO emitting region into context to the dust disk, we need to estimate its possible location. From our determination of the stellar distance, the disk inclination, and the size of the warm silicate dust region visible in the N-band, we can conclude that the majority of the dust emitting at these wavelengths must be located at a distance of 28.4 ± 7.8 AU. The presence of the silicate bands around 10 μm is a clear indication for oxygen-rich dust, which is expected because CPD−52 9243 is a massive star. This places the CO emitting region with its slightly higher temperature of about 2400 K to distances a little (but not very much) closer to the star. Consequently, the very low velocity of the CO gas allows us to conclude that the CO emission most probably originates from a Keplerian rotating disk rather than from an equatorially outflowing wind, simply based on kinematical arguments.

To estimate the possible inner edge of the dusty disk, we computed the evaporation distance of silicate grains assuming that the grains are spheres with a maximum radius of about 1 μm. The typical evaporation temperature is 1600 K, which delivers an evaporation distance of r_{evap}(Si) = 14.7 AU. This distance can be regarded as a plausible value for the inner edge of the dusty disk.

Using the stellar masses obtained in Sect. 3.1, we computed the Keplerian rotation velocities as a function of distance, which are shown in the top panel of Fig. 11. The dotted lines give the range of the observed (corrected for inclination) rotation velocities. The bottom panel of this figure shows the minimum and maximum ranges (solid line) of the outer edge of the CO emitting region as function of the inner edge, obtained from the minimum and maximum emitting areas (as listed in Table 5). The vertical dashed lines mark (i) the evaporation distance of the silicate dust; and (ii) the minimum distance of the CO emitting region, defined by the maximum observed Keplerian rotation velocity (from the top panel). The dotted line shows just the 1:1 correlation. The real distance of the CO emitting region should be located somewhere between these two dashed bordering lines.

4. Discussion and conclusions

Based on our combined set of data taken in the optical, near- and mid-IR regions, we derived the stellar parameters of CPD−52 9243 and some properties of its circumstellar environment. CPD−52 9243 is a B[e] supergiant located at ~3.4 kpc from the Sun. It has a stellar mass of 17–18 solar masses and a luminosity relative to the Sun of $\log L/L_{\odot} = 5$.

High angular resolution interferometric measurements obtained with VLTI/MIDI provide strong support for the presence of a dusty disk-like (or ring) structure around CPD−52 9243, with an upper limit for the inner edge around 8 mas (~28 AU). The disk has an orientation on the plane of the sky of ~60° and an inclination to line of sight of ~46°. At present, we cannot give a detailed description of the structure of the dusty environment because our interferometric analysis is based on a few points in the UV-plane (only four sets of visibilities). We could determine that the dusty structure surrounds a narrow CO gaseous ring in

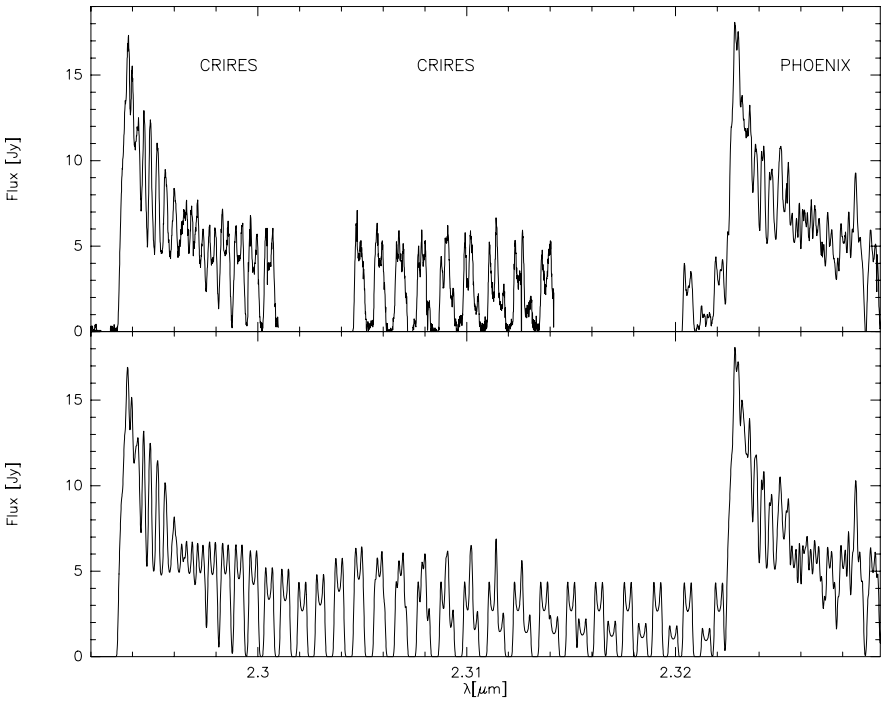

Fig. 10. *Top panel*: observed flux-calibrated CO bands. *Botton panel*: best-fitting model, see details in Table 5.

Table 5. Parameters for the best-fitting CO model.

T_{CO} [K]	N_{CO} [cm^{-2}]	i [°]	v_{rot} [km s^{-1}]	A_{CO} [AU^2]
2400	4×10^{22}	46.1	36	9.6
±100	$\pm 1 \times 10^{22}$	±7	±4	±5.7

Notes. The second row gives the errors for each parameter.

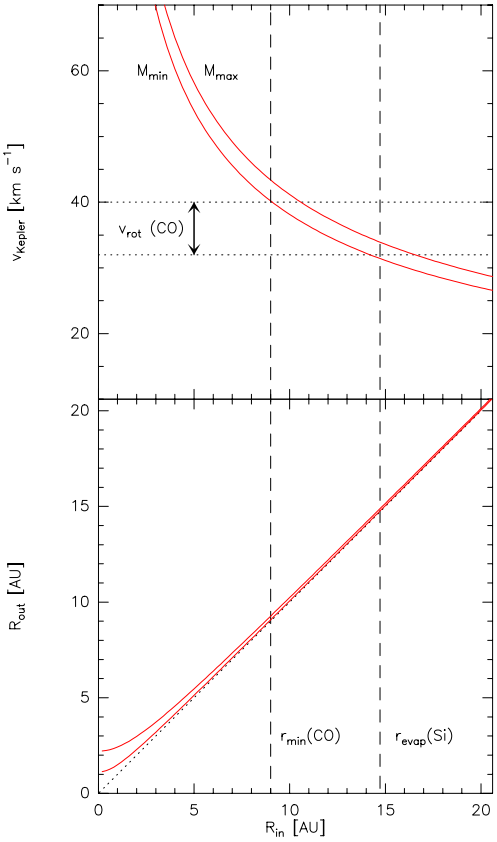

Fig. 11. *Top panel*: Keplerian rotation velocity distribution for the minimum and maximum stellar masses. The minimum inner edge of the CO ring follows from the observed inclination corrected velocity. *Bottom panel*: evaporation distance of silicate dust as upper limit for the inner edge of the CO ring. For details see text.

Keplerian rotation. The CO emitting ring is confined to a very narrow ring, where R_{out} is not much larger than R_{in}, and the low temperature of the CO gas might hint towards a detached disk with the CO emitting ring as the inner edge of the complete gaseous and dusty disk. Finally, the optical line spectrum evidences a strong and rapid wind outflow of about −280 km s^{-1} (corrected by the inclination angle). Therefore, the existence of regions with quite different kinematical structures is consistent with a model with a Keplerian disk and a polar wind.

We want to draw the attention to the fact that the CO band emission always traces the hottest ring of the molecular gas. The temperature of only 2400±100 K found from our modeling turns out to be rather cold compared to the dissociation temperature of CO, which is of the order of 5000 K. Similarly, cold CO rings have recently been found to surround two B[e] supergiants in the Large Magellanic Cloud (Liermann et al. 2010). For those stars, a maximum CO temperature of 2800 K was also derived. Liermann et al. (2010) interpreted the lack of hot CO gas around these luminous stars as the result of a detached ring surrounding the stars, rather than a disk reaching to much smaller distances from the star. The presence of a detached ring rather than of a disk was also recently suggested by Kraus et al. (2010) for another B[e] supergiant in the Small Magellanic Cloud, based on an optical analysis of its variety of the numerous emission lines. Hence, such an interpretation might also hold for the disk/ring of CPD−52 9243 due to the absence of hot CO gas close to the star.

The presence of a detached cold CO ring around the star, and the fact that the star presents irregular light variations of about hundreds of days, could be due to a truncation of the inner disk caused by a companion, located possibly interior to the disk rim, clearing the center of the system. In the last years, the number of observations supporting the hypothesis that the

B[e] phenomenon behavior could also be attributed to binarity has increased dramatically. Recently, binary components around B[e] stars were confirmed using interferometry techniques in V 921 Sco (Kraus et al. 2012), HD 327083 (Wheelwright et al. 2012a,b) and HD 62623 (Millour et al. 2011). Mass exchange processes and wind interactions play an important role not only in the evolution of stars but also in the formation of gaseous and dusty circumstellar disks. This is the case of the hydrogen deficient supergiant υ Sgr which also exhibits an important amount of dust (Bonneau et al. 2011; Netolický et al. 2009).

To confirm the possible hypothesis of binarity in CPD-52 9243 and better constrain its disk geometry, more spectroscopic and, especially, interferometric data are necessary. New high-resolution observations will enable us to use not only more complex analytical models, but also physical models.

Acknowledgements. L.C. acknowledges financial support from the Agencia de Promoción Científica y Tecnológica (BID 1728 OC/AR PICT 0885), from CONICET (PIP 0300), and the Programa de Incentivos G11/109 of the Universidad Nacional de La Plata, Argentina. M.B.F. acknowledges Conselho Nacional de Desenvolvimento Científico e Tecnológico (CNPq-Brazil) for the post-doctoral grant. I.A. acknowledges financial support from a posdoctoral fellowship of CONICET. Also thanks to Alan Spang for helping in the MIDI reduction process and all the staff at the Observatoire de la Côte d'Azur, GRASSE. M.K. acknowledges financial support from GA ČR under grant number 209/11/1198. The Astronomical Institute Ondřejov is supported by the project RVO:67985815. S.K. and M.C. thanks the support of GEMINI-CONICYT project N° 32090006, CONICYT-FONDECYT project N° 3120037, CONICYT Capital Humano Avanzado project N° 7912010046, and Centro de Astrofísica de Valparaíso. M.C. also thanks the financial support from CONICYT, Departamento de Relaciones Internacionales "Programa de Cooperación Científica Internacional" CONICYT/MINCYT 2011-656 and from Centro de Astrofísica de Valparaíso. M.L.A. acknowledges finantial support from MINCYT-CONICYT (project CH/11/03). Financial support for International Cooperation of the Czech Republic (MŠMT, 7AMB12AR021) and Argentina (Mincyt-Meys, ARC/11/10) is acknowledged.

References

Angel, J. R. P. 1969, ApJ, 158, 219
Bjorkman, J. E., & Cassinelli, J. P. 1993, ApJ, 409, 429
Bonneau, D., Chesneau, O., Mourard, D., et al. 2011, A&A, 532, A148
Brown, J. C., & McLean, I. S. 1977, A&A, 57, 141
Curé, M. 2004, ApJ, 614, 929
Curé, M., Rial, D. F., & Cidale, L. 2005, A&A, 437, 929
Domiciano de Souza, A., Driebe, T., Chesneau, O., et al. 2007, A&A, 464, 81
Ekström, S., Georgy, C., Eggenberger, P., et al. 2012, A&A, 537, A146
Jaffe, W. J. 2004, in SPIE Conf. Ser. 5491, ed. W. A. Traub, 715
Kaeufl, H.-U., Ballester, P., Biereichel, P., et al. 2004, in SPIE Conf. Ser. 5492, eds. A. F. M. Moorwood, & M. Iye, 1218
Kozok, J. R. 1985, A&AS, 62, 7
Kraus, M. 2009, A&A, 494, 253
Kraus, M., Krügel, E., Thum, C., & Geballe, T. R. 2000, A&A, 362, 158
Kraus, M., Borges Fernandes, M., & de Araújo, F. X. 2010, A&A, 517, A30
Kraus, S., Calvet, N., Hartmann, L., et al. 2012, ApJ, 752, 11
Lamers, H. J. G., & Pauldrach, A. W. A. 1991, A&A, 244, L5
Lamers, H. J. G. L. M., Zickgraf, F.-J., de Winter, D., Houziaux, L., & Zorec, J. 1998, A&A, 340, 117
Leinert, C., van Boekel, R., Waters, L. B. F. M., et al. 2004, A&A, 423, 537
Lenz, P., & Breger, M. 2005, Commun. Asteroseismol., 146, 53
Liermann, A., Kraus, M., Schnurr, O., & Fernandes, M. B. 2010, MNRAS, 408, L6
Lopes, D. F., Damineli Neto, A., & de Freitas Pacheco, J. A. 1992, A&A, 261, 482
Magalhães, A. M. 1992, ApJ, 398, 286
Magalhães, A. M., Melgarejo, R., Pereyra, A., & Carciofi, A. C. 2006, in Stars with the B[e] Phenomenon, eds. M. Kraus, & A. S. Miroshnichenko, ASP Conf. Ser., 355, 147
McClure-Griffiths, N. M., & Dickey, J. M. 2007, ApJ, 671, 427
McGregor, P. J., Hyland, A. R., & Hillier, D. J. 1988, ApJ, 324, 1071
Melgarejo, R., Magalhães, A. M., Carciofi, A. C., & Rodrigues, C. V. 2001, A&A, 377, 581
Millour, F., Meilland, A., Chesneau, O., et al. 2011, A&A, 526, A107
Miroshnichenko, A. S. 2006, in Stars with the B[e] Phenomenon, eds. M. Kraus, & A. S. Miroshnichenko, ASP Conf. Ser., 355, 365
Miroshnichenko, A. S., Bergner, Y. K., Mukanov, D. B., & Shejkina, T. A. 1995, Ap&SS, 224, 519
Netolický, M., Bonneau, D., Chesneau, O., et al. 2009, A&A, 499, 827
Oudmaijer, R. D., & Drew, J. E. 1999, MNRAS, 305, 166
Pauldrach, A., Puls, J., & Kudritzki, R. P. 1986, A&A, 164, 86
Porter, J. M. 2003, A&A, 398, 631
Swings, J. P. 1981, A&A, 98, 112
Wheelwright, H. E., de Wit, W. J., Oudmaijer, R. D., & Vink, J. S. 2012a, A&A, 538, A6
Wheelwright, H. E., de Wit, W. J., Weigelt, G., Oudmaijer, R. D., & Ilee, J. D. 2012b, A&A, 543, A77
Whitelock, P. A., Feast, M. W., Roberts, G., Carter, B. S., & Catchpole, R. M. 1983, MNRAS, 205, 1207
Winkler, H., & Wolf, B. 1989, A&A, 219, 151
Zickgraf, F.-J. 1998, Habilitation Thesis, Heidelberg University
Zickgraf, F.-J., Wolf, B., Stahl, O., Leitherer, C., & Klare, G. 1985, A&A, 143, 421